

Room-temperature scavengers for macromolecular crystallography: increased lifetimes and modified dose dependence of the intensity decay

Adam I. Barker,^{a‡} Robert J. Southworth-Davies,^{a‡} Karthik S. Paithankar,^a
Ian Carmichael^b and Elspeth F. Garman^{a*}

^aLaboratory of Molecular Biophysics, Department of Biochemistry, University of Oxford, South Parks Road, Oxford OX1 3QU, UK, and ^bNotre Dame Radiation Laboratory, University of Notre Dame, IN 46556, USA. E-mail: elspeth.garman@bioch.ox.ac.uk

The advent of highly intense wiggler and undulator beamlines has reintroduced the problem of X-ray radiation damage in protein crystals even at cryogenic temperatures (100 K). Although cryocrystallography can be utilized for the majority of protein crystals, certain macromolecular crystals (*e.g.* of viruses) suffer large increases in mosaicity upon flash cooling and data are still collected at room temperature (293 K). An alternative mechanism to cryocooling for prolonging crystal lifetime is the use of radioprotectants. These compounds are able to scavenge the free radical species formed upon X-ray irradiation which are thought to be responsible for part of the observed damage. Three putative radioprotectants, ascorbate, 1,4-benzoquinone and 2,2,6,6-tetramethyl-4-piperidone (TEMP), were tested for their ability to prolong lysozyme crystal lifetimes at 293 K. Plots of relative summed intensity against dose were used as a metric to assess radioprotectant ability: ascorbate and 1,4-benzoquinone appear to be effective, whereas studies on TEMP were inconclusive. Ascorbate, which scavenges OH• radicals ($k_{\text{OH}} = 8 \times 10^9 \text{ M}^{-1} \text{ s}^{-1}$) and electrons with a lower rate constant ($k_{\text{e-(aq)}} = 3.0 \times 10^8 \text{ M}^{-1} \text{ s}^{-1}$), doubled the crystal dose tolerance, whereas 1,4-benzoquinone, which also scavenges both OH• radicals ($k_{\text{OH}} = 1.2 \times 10^9 \text{ M}^{-1} \text{ s}^{-1}$) and electrons ($k_{\text{e-(aq)}} = 1.2 \times 10^{10} \text{ M}^{-1} \text{ s}^{-1}$), offered a ninefold increase in dose tolerance at the dose rates used. Pivotaly, these preliminary results on a limited number of samples show that the two scavengers also induced a striking change in the dose dependence of the intensity decay from a first-order to a zeroth-order process.

1. Introduction

Radiation damage in macromolecular crystallography is an increasingly important problem, since the structural changes induced by such damage result in non-isomorphism, which is thought to be a major cause of unsuccessful MAD (multiple-wavelength anomalous dispersion) structure determinations. In addition, radiation-damage-induced structural changes can affect the biological properties of macromolecules, *e.g.* change the oxidation state of metal ions in structural/active sites and cause decarboxylation of glutamate and aspartate residues. In such circumstances, separating radiation damage from enzymatic mechanism can be extremely difficult and casts doubt on

the validity of biological conclusions drawn from crystal structures (Ravelli & Garman, 2006).

Radiation damage is a result of the deposition of energy into the macromolecule owing to the inelastic interactions between X-rays and matter. The damage can be classified as primary or secondary in nature. Primary damage is the ionization of an atom owing to photoelectric absorption or Compton scattering, whereas secondary damage is the formation of up to 500 low-energy secondary electrons per primary absorption event which are able to diffuse and induce further ionization and excitation events, with the photoelectron having a mean track length of a few micrometres (for 12 keV photons) (O'Neill *et al.*, 2002). Damage can also be classified as direct if it occurs on a protein molecule, or indirect if the radiation is absorbed by the surrounding solvent and the

[‡] These authors contributed equally to this work.

radiation damage

reactive species formed subsequently interact with the protein (Murray & Garman, 2002). The radiation damage manifests itself as a global decrease in the intensity of the diffraction pattern, with higher resolution reflections being the first to fade. At 100 K, site-specific structural damage also occurs in a well defined order, with disulfide bonds and the γ -carboxylate groups of amino acids (*e.g.* glutamate) being particularly susceptible (Burmeister, 2000; Ravelli & McSweeney, 2000; Weik *et al.*, 2000).

The first systematic study of radiation damage was carried out at room temperature on sperm whale myoglobin (Blake & Phillips, 1962). From their study it was concluded that the extent of damage was proportional to the dose of absorbed X-rays, and they were able to calculate that one 8 keV photon disrupts around 70 protein molecules, and disorders a further 90 for doses up to 0.2 MGy. In addition, it was demonstrated that the observed intensity decay with dose was characterized by a first-order (exponential) process, which is in contrast to the zeroth-order (linear) intensity decay with dose observed at 100 K (Owen *et al.*, 2006).

Recently, it was found that at 293 K the dose tolerated by a lysozyme protein crystal is dependent upon the dose rate according to a positive linear relationship; a 60% increase in dose rate gave a fourfold increase in lysozyme crystal dose tolerance. The effect was observed over a short range of dose rate (6–10 Gy s⁻¹) (Southworth-Davies *et al.*, 2007) and further studies analysing a wider range of dose rates and different proteins are ongoing (Armstrong, 2008).

Can radiation damage be prevented? Unfortunately, primary damage is a consequence of physics and cannot be avoided. However, direct and indirect primary damage results in the formation of mobile species: electrons and positive holes in the case of direct processes, and the species such as those depicted in Fig. 1 from water radiolysis in the case of indirect processes. Damage by X-rays and other ionizing radiation has been found by electron spin resonance (ESR) to proceed *via* the formation and propagation of free radicals (Swartz & Swartz, 1983). Thus attempting to neutralize or reduce the mobility of such radical species provides a potential avenue to reduce radiation damage.

The first attempt to mitigate radiation damage arose from experiments which highlighted the importance of temperature in the damage process, when it was shown that the resolution of the diffraction was limited by temperature-dependent dynamic disorder in the protein ribonuclease II (King, 1958). Haas & Rossmann (1970) then monitored two particular

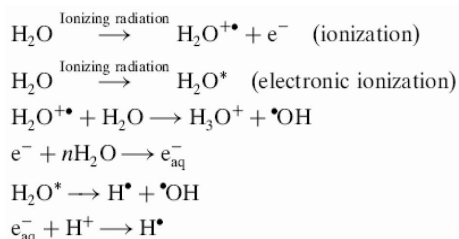


Figure 1
Species produced by indirect primary damage to water (Ward, 1988).

reflections from dog fish lactate dehydrogenase crystals at 298 K and 198 K and it was found that the intensity loss with accumulated dose was much greater at 298 K. These observations eventually led to the development of macromolecular crystallography cryocooling techniques (Hope, 1988; Teng, 1990; Garman & Schneider, 1997; Rodgers, 1997; Garman, 1999; Garman & Owen, 2006). Protein crystals are now routinely flash-cooled to 77 K or 100 K, and held at 100 K during most diffraction experiments.

Several published studies have analysed the mobility of the various species formed upon X-ray exposure and they help to explain the effectiveness of cryocooling. Protons are only known to become mobile in amorphous ice at ~ 115 K (Fisher & Devlin, 1995) and, although OH \bullet radicals are trapped at 100 K in ice crystals (Symons, 1999), they have also been reported to be mobile at 77 K in a glass of DNA (Lange *et al.*, 1995). According to the ESR measurements of Jones *et al.* (1987), at 77 K positive holes in proteins are rapidly trapped, forming amido radicals on the protein backbone chain, whereas the electrons produced by inelastic interactions have significant mobility. Rao *et al.* (1983) showed that electrons added to proteins at 77 K are able to move efficiently until they encounter S–S bonds, where they are trapped.

Although cryocooling substantially improves the situation, damage is still observed in cryocooled protein crystals. Such damage was first described by Gonzalez *et al.* (1992) and further studied by Gonzalez & Nave (1994) who observed measurable decay of diffraction patterns at 100 K from lysozyme crystals. This fact, coupled with the observation of specific damage, suggests a possible mitigation strategy employing radioprotectants and free radical scavengers.

Radioprotectants are compounds that either react with secondary radicals before they have a chance to damage the protein, or interact with already damaged sites in the protein. Radical scavengers intercept the highly reactive radical species formed in the solvent surrounding the protein, producing less reactive radicals of lower mobility, which have decreased potential for damaging the protein.

For protein crystals at room temperature the first studies on free-radical scavengers were carried out by soaking 2–30 mM styrene into radiation-sensitive immunoglobulin crystals. An increase in resolution from 5.5 Å to 4 Å, and a tenfold increase in effective crystal lifetime was observed (Zaloga & Sarma, 1974; Sarma & Zaloga, 1975). However, as the styrene concentration increased, diffraction quality deteriorated, probably owing to polymerization of the styrene.

Cascio *et al.* (1984) tested the effect of replacing native mother liquor with comparable solutions which contained in addition 10–20% by weight polyethylene glycol (PEG) of molecular weight (MW) 4000 or 20000. It was found that radiation damage was reduced in the three proteins tested: α -amylase, canavalin and fructose-1,6-diphosphatase. For example, for α -amylase, certain reflections suffered an intensity reduction of 90% following a 20 h exposure to 1.54 Å X-rays. However, upon addition of 12% PEG MW 20000, crystals survived for 90 h in the X-ray beam, showing decay in the diffraction intensity of no more than 10%.

After this early work at room temperature, little was done to further scavenger investigations until the advent of third-generation synchrotron sources at which radiation damage was observed even at 100 K.

Murray & Garman (2002) studied the use of styrene and ascorbate as radioprotectants in cryocrystallography by analysing the rate of intensity decay of lysozyme crystals, but styrene had no observable effects; in addition, it is toxic and difficult to work with, and no further investigations with it have been undertaken. However, crystals grown with 0.5 M ascorbate were less susceptible to radiation damage, as evidenced from analysis of specific structural damage in electron density maps. The ascorbate co-crystal structures also showed much lower increases in refined atomic *B* factors compared with those of the native. The study involved the use of a microspectrophotometer, which showed the presence of a 400 nm peak in native crystals, but an absence of such a peak in ascorbate co-crystals; this peak has been attributed to a disulfide radical anion (Weik *et al.*, 2002).

Betts (2003) soaked 0.5 M ascorbate for 12 h into avian influenza virus N9 neuraminidase crystals, and, by inspection of electron density maps, showed that at 100 K the residues on the exterior of the protein were protected, but not those on the inside of the hollow ball formed by the N9 protein tetramers in the crystals, which grow in space group *I432*. This suggested a lack of penetration by the ascorbate molecules. Betts also tested the use of 0.5 M glucose as a radioprotectant, again by soaking into N9 crystals, but interestingly this appeared to increase the damage rate. Nicotinic acid and 5,5'-dithiobis-2-nitrobenzoic acid (DTNB) have been found to act as effective free radical scavengers when used on crystals of HEWL, thaumatin and elastase at 100 K (Kauffmann *et al.*, 2006). Interestingly, for HEWL and elastase, nicotinic acid protected disulfides but not glutamates, but, for DTNB, disulfides were found not to be protected although aspartates were, suggesting that different mitigating mechanisms were at work.

Subsequently, an online microspectrophotometer (McGeehan *et al.*, 2009) was employed to analyse the disulfide radical anion 400 nm peak (Armstrong, 1990) during irradiation of cryoprotected 0.1 M disulfide test systems held at 100 K, with and without the presence of potential radioprotectants. The experiments used cysteine (S—H bond), cystine (S—S bond), and oxidized α -lipoic acid (S—S) to model thiol (S—H) and disulfide (S—S) groups, respectively. Ascorbate was shown to be an effective radioprotectant at concentrations between 0.3 M and 1 M since it quenched the appearance of the 400 nm peak for all the disulfide test systems. Similarly, TEMP (2,2,6,6-tetramethyl-4-piperidone) was effective on the oxidized α -lipoic acid, but not on the cystine; the reason for this is unknown. 1,4-Benzoquinone was effective on both test systems, but became ineffective when the concentration used was less than 0.4 M (Southworth-Davies & Garman, 2007). Interestingly, and contrary to the results of Cascio *et al.* (1984) at room temperature, PEG showed no positive effects as a radioprotectant. Southworth-Davies & Garman suggested that the earlier results with

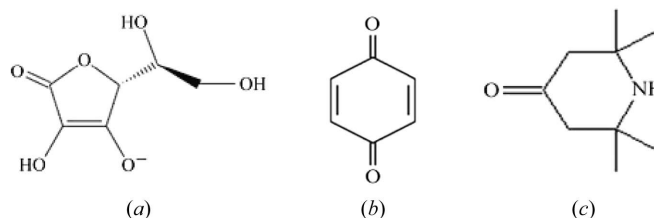


Figure 2

The three radioprotectants tested in this study: (a) ascorbate, (b) 1,4-benzoquinone and (c) TEMP.

PEG may have been due to dehydration or a polymerization effect.

It should be noted that the concentrations of scavengers being utilized in the above experiments are orders of magnitude greater than those often employed in typical radiation chemistry scavenging studies.

Although recent research has investigated the utility of radioprotectants at 100 K, few studies have analysed their potential use at 293 K. Use of room-temperature protein crystallography is particularly critical for the study of viruses, where flash-cooling often results in large increases in crystal mosaicity which jeopardize successful data collection. In the experiments reported below, the effect of three potential radioprotectants [sodium ascorbate, 1,4-benzoquinone and TEMP (Fig. 2)] on the lifetime of lysozyme crystals at 293 K was investigated. The change in relative summed intensity (I/I_0) and on the specific structural damage with respect to the dose [the energy deposited (J) per kg of crystal] was monitored. The dose required to reduce the summed intensity for a complete data set to half of its original value, $D_{1/2}$, was determined from plots of the intensity decay against the absorbed dose, and for the effective scavengers the radioprotectant enhancement factor, $D_e = D_{1/2}(\text{with scavenger})/D_{1/2}(\text{native})$, was derived.

2. Materials and methods

2.1. Crystallization

Chicken egg-white lysozyme (HEWL) was obtained from Merck Biosciences and crystallized by the hanging-drop vapour diffusion method. The well solution (400 μ l) was composed of 4–8% w/v NaCl in 100 mM sodium acetate at pH 4.5. The required pH was obtained with 1 M HCl by using a calibrated Schott CG840 pH meter. The protein solution (1 ml) contained 30 mg ml⁻¹ HEWL in 100 mM sodium acetate, and the suspended drop contained 1 μ l of well solution and 1 μ l of protein solution. Crystals grew in space group *P4₃2₁2*, and ranged in size from 100 \times 100 \times 100 μ m to 300 \times 300 \times 300 μ m. Those of dimensions 200 \times 200 \times 200 μ m were selected for the study where possible (see Tables 1a–d). Crystals were also grown in the presence of scavengers (Sigma): sodium ascorbate (A7631), 1,4-benzoquinone (B10358) and TEMP (459119) by addition of an equal volume of 1 M scavenger to the well solution (1,4-benzoquinone and

Table 1
Data collection parameters.

(a)	NAT1	NAT2	ASC1	ASC2
Beam	MicroStar	MicroStar	MicroStar	MicroStar
Energy (keV)	8.05	8.05	8.05	8.05
Number of images per data set	45	45	90	90
$\Delta\varphi$ (°)	1	1	1	1
Number of oscillations	1	1	1	1
Total angle (°)	45	45	90	90
Exposure time / image (s)	60	120	120	120
Number of data sets	8	5	4	5
Detector distance (mm)	170	170	170	170
Crystal size, x, y, z (mm)	$0.2 \times 0.2 \times 0.2$	$0.2 \times 0.1 \times 0.05$	$0.18 \times 0.18 \times 0.05$	$0.2 \times 0.1 \times 0.1$
Crystal volume (mm ³)	8.0×10^{-3}	1.0×10^{-3}	1.6×10^{-3}	2.0×10^{-3}
Slit size, $v \times h$ (mm)	1×1	1×1	1×1	1×1
Beam size, $v \times h$ (mm)	0.6×0.5	0.6×0.5	0.6×0.5	0.6×0.5
Dose rate (Gy s ⁻¹)	6.4	12.8	6.0	6.0

(b)	NAT3	ASC3
Beamline	ID14-2 (ESRF)	ID14-2 (ESRF)
Energy (keV)	13.29	13.29
Number of images per data set	90	90
$\Delta\varphi$ (°)	1	1
Number of oscillations	1	1
Total angle (°)	90	90
Exposure time / image (s)	1	1
Number of data sets	7	7
Detector distance (mm)	184	186
Crystal size, x, y, z (mm)	$0.2 \times 0.2 \times 0.2$	$0.2 \times 0.2 \times 0.2$
Crystal volume (mm ³)	8×10^{-3}	8×10^{-3}
Slit size, $v \times h$ (mm)	0.1×0.1	0.1×0.1
Beam size, $v \times h$ (mm)	0.1×0.1	0.1×0.1
Dose rate (Gy s ⁻¹)	2800	2800

(c)	NAT4	QUIN1	QUIN2
Beam	MicroStar	MicroStar	MicroStar
Energy (keV)	8.05	8.05	8.05
Number of images per data set	45	180	90
$\Delta\varphi$ (°)	1	0.5	1
Number of oscillations	1	1	1
Total angle (°)	45	90	90
Exposure time / image (s)	180	300	600
Number of data sets	7	6	3
Detector distance (mm)	175	175	175
Crystal size, x, y, z (mm)	$0.2 \times 0.2 \times 0.2$	$0.2 \times 0.2 \times 0.1$	$0.2 \times 0.2 \times 0.1$
Crystal volume (mm ³)	8.0×10^{-3}	4.0×10^{-3}	4.0×10^{-3}
Slit size, $v \times h$ (mm)	1×1	1×1	1×1
Beam size, $v \times h$ (mm)	0.6×0.5	0.6×0.5	0.6×0.5
Dose rate (Gy s ⁻¹)	5.7	6.4	6.0

(d)	NAT5	NAT6	TEMP1	TEMP2
Beam	Rigaku RU200H	RU200H	RU200H	RU200H
Energy (keV)	8.05	8.05	8.05	8.05
Number of images per data set	90	45	90	45
$\Delta\varphi$ (°)	1	1	1	1
Number of oscillations	1	1	1	1
Total angle (°)	90	45	90	45
Exposure time / image (s)	180	180	180	300
Number of data sets	6	7	4	5
Detector distance (mm)	175	175	175	170
Crystal size, x, y, z (mm)	$0.15 \times 0.1 \times 0.05$	$0.2 \times 0.1 \times 0.1$	$0.15 \times 0.15 \times 0.05$	$0.15 \times 0.15 \times 0.05$
Crystal volume (mm ³)	7.5×10^{-4}	2.0×10^{-3}	1.1×10^{-3}	1.1×10^{-3}
Slit size, $v \times h$ (mm)	1×1	1×1	1×1	1×1
Beam size, $v \times h$ (mm)	0.45×0.45	0.45×0.45	0.45×0.45	0.45×0.45
Dose rate (Gy s ⁻¹)	4.6	4.8	4.5	4.8

TEMP) in the volume ratio 1:1 and 1 M scavenger pipetted on top of the crystallization drop (ascorbate) again in the volume ratio 1:1 to give a final concentration of at least 0.5 M scavenger in the crystal.

2.2. Crystal mounting

The MiTeGen room-temperature mounting system (Kalinin *et al.*, 2005) was used, in which a polyethylene terephthalate (PET) tube with a small volume of mother liquor (with/without scavenger) pipetted into the top (rather than a quartz capillary) is placed over the crystal held in a premounted rayon cryo-loop. This PET tube was more easily cut to the required length than was a quartz capillary, and both ends of the plastic tube were sealed with vacuum grease to prevent dehydration of the crystal. Rayon cryoloops which were closely matched to the crystal dimensions were used for all the measurements.

2.3. Introduction of the scavengers into the crystals

For experiments with sodium ascorbate (ASC), co-crystals were grown. However, co-crystals produced by adding 1 M 1,4-benzoquinone and 1 M TEMP were found to diffract poorly, and hence soaking was carried out by pipetting an equal volume of 1 M scavenger solution onto the crystallization drop containing native crystals on the cover slip, and then subsequently placing the cover slip back over the well solution and leaving the crystals to soak for a defined period of time. The scavenger concentration in the drop was thus approximately 0.5 M. For 1,4-benzoquinone, crystals 1 (QUIN1) and 2 (QUIN2) were soaked for three days and seven days, respectively, and for TEMP, crystals 1 (TEMP1) and 2 (TEMP2) were soaked for three hours and five days, respectively.

2.4. Data collection

Room-temperature X-ray data were collected using two in-house

rotating copper anode generators: a Bruker AXS Microstar and a Rigaku RU200H producing 1.54 Å (8.05 keV) X-rays, and both equipped with MAR345 imaging plate detectors. A summary of the data collection parameters is given in Tables 1(a)–1(d).

The ascorbate (two native crystals: NAT1 and NAT2; and two co-crystallized samples: ASC1, ASC2) and 1,4-benzoquinone (one native NAT4 and two soaked crystals: QUIN1, QUIN2) diffraction data were collected using the Microstar. TEMP diffraction data (two native crystals: NAT5 and NAT6; two soaked crystals: TEMP1 and TEMP2) were collected on the Rigaku RU200H.

Data for one native (NAT3) and one ascorbate-soaked (ASC3) crystal were collected, again at room temperature, at the European Synchrotron Radiation Facility (ESRF) in Grenoble, France.

For each pair of native and scavenger treated crystals, the dose rates were kept as near as possible constant, since dose rate is known to affect crystal dose tolerance at room temperature (Southworth-Davies *et al.*, 2007). However, matching the dose rates for the different crystals was not trivial as there are many variables, not all easy to control accurately. For the ascorbate data, the dose rates were 6.0 Gy s⁻¹ (NAT1), 6.4 Gy s⁻¹ (ASC1 and ASC2), 12.8 Gy s⁻¹ (NAT2) and 2800 Gy s⁻¹ (NAT3 and ASC3). For the 1,4-benzoquinone, the rates were 6.0 Gy s⁻¹ (NAT1), 5.7 Gy s⁻¹ (NAT4), 6.4 Gy s⁻¹ (QUIN1) and 6.0 Gy s⁻¹ (QUIN2). The dose rates for the TEMP data were lower since they were collected on the Rigaku rather than the MicroStar in-house source, and were 4.6 Gy s⁻¹ (NAT5), 4.8 Gy s⁻¹ (NAT6), 4.5 Gy s⁻¹ (TEMP1) and 4.8 Gy s⁻¹ (TEMP2).

2.5. Dose calculations

The program *RADDOSE* was used to calculate the absorbed dose [in Gy (J kg⁻¹)]. The program uses physical and chemical information about the crystal (atomic content, size) to calculate the absorption coefficient of the crystal (μ_{abs}) and knowledge of the beam parameters (size, energy, profile, flux, position) to calculate the dose absorbed. Further details of the *RADDOSE* calculation can be found in the literature (Murray *et al.*, 2004; Paithankar *et al.*, 2009) and will not be repeated here.

The detailed methods and calibrations used to calculate the in-house beam (size, profile and intensity) and the crystal parameters (size) have been described previously (Southworth-Davies *et al.*, 2007).

Analysis of the error on the dose calculation shows that the contributions are largely systematic, affecting all doses and dose rates by the same proportion. These include errors in the beam profile and the beam size (total of $\pm 6\%$ in x and y), and a possible systematic error on the diode calibration [estimated at 5% from cross calibration against two other calibrated diodes (Owen *et al.*, 2009)]. Estimated uncertainties in measured crystal sizes give comparatively small errors in the dose, as if the dimensions are smaller (or larger) than in reality; the cross section to photon flux is reduced (or

increased), but the volume also decreases (or increases) resulting in almost the same calculated dose.

2.6. Data reduction, processing and structure refinement

The CCP4 programming suite (Collaborative Computational Project, Number 4, 1994) was used for processing all data sets. Autoindexing and integration (between 40 Å and 2 Å resolution) were carried out using *MOSFLM* (Leslie, 2006). *SCALA* (Evans, 2006) was used to scale together multiple observations of reflections, merge multiple observations into an average intensity for a data set, and assign identical test reflections (for the R_{free} set) for every data set. In order to convert intensities into structure factor amplitudes the program *TRUNCATE* (French & Wilson, 1978) was utilized. The files output from *SCALA* were merged together using the program *CAD*, and Wilson scaling was used to scale the data sets from one crystal series to the others *via* the program *SCALEIT* (Howell & Smith, 1992).

$\langle I_{\text{mean}} \rangle$ values, defined as the mean diffracting power of a crystal for a particular data set, were determined by summing the mean intensity of unweighted scaled reflections on each image (I_{mean}) over all images in a data set and dividing by the number of images, as output by *SCALA*. Since some of the first scavenger data sets had a different absorbed dose from the corresponding natives, normalization was required to compare the relative decay. The intensity normalization of the $\langle I_{\text{mean}} \rangle$ values to that of the first native data set for these pairs was carried out in the following way.

(i) The $\langle I_{\text{mean}} \rangle$ values of the first native data set (NAT1, NAT3) were normalized to 1.0.

(ii) The ASC and QUIN $\langle I_{\text{mean}} \rangle$ plots *versus* dose were fitted to straight lines, and extrapolated back to the dose corresponding to the first native data set.

(iii) The extrapolated points [indicated by asterisks (*) in Tables 2 and 3] were then normalized to 1.0 and thus all samples had the same dose for the normalization of the first point.

(iv) For NAT2 (collected at double the dose rate of NAT1), the first data set was normalized to unity, but ASC1 and ASC2 were not extrapolated to this point: the first data set of NAT1 was used for the extrapolation, since the dose rates were almost the same for NAT1, ASC1 and ASC2.

Although this procedure neglects any improvement of the radiation resistance of the scavenger crystal during the first data set, after tests it was judged to cause a substantially smaller error than extrapolating the exponentials back to zero dose for the normalization. Ideally, all first data sets would be for the same absorbed dose, but owing to the crystal orientation in the loop it was not always possible to obtain a complete data set for the same absorbed dose, and $\langle I_{\text{mean}} \rangle$ can only meaningfully be used as a metric if it is for complete data sets. The error in $\langle I_{\text{mean}} \rangle$ was estimated to be less than $\pm 3\%$.

Molecular replacement was unnecessary in this study because the starting Protein Data Bank model of HEWL was derived from a crystal in the same space group and had the same unit cell, so refinement with the existing phases was

Table 2

Data statistics from the native HEWL crystals NAT1 and NAT2, and ascorbate co-crystals ASC1 and ASC2 collected in-house.

Results for native NAT3 and ascorbate ASC3 HEWL data collected at the ESRF are also shown. The resolution range in all cases was 40.00–2.00 Å (2.10–2.00 Å outer shell). For all these data sets the completeness was greater than 98%. The asterisks (*) at the beginning of the ASC1, ASC2 and ASC3 entries denote the virtual normalized intensity point at the same dose as for the first data set of NAT1 (for ASC1 and ASC2) and NAT3 (for ASC3), as described in the text. The (–) sign represents values above 0.6. $\langle I_{\text{mean}} \rangle$ is the diffracting power of a crystal for a particular data set, determined by summing the mean intensity of unweighted scaled reflections on each image (I_{mean}) over all images in a data set and dividing by the number of images. $R_{\text{meas}} = \{ \sum_h [n_h / (n_h - 1)]^{1/2} \sum_i |I_h - I_{h,i}| / \sum_h \sum_i I_{h,i} \}$ where $I_h = (1/n_h) \sum_i I_{h,i}$.

Crystal	DS	Dose (MGy)	Unique reflections	Multiplicity	$I/\sigma(I)$	R_{meas}	Wilson B value (Å ²)	$\langle I_{\text{mean}} \rangle$	I/I_0
NAT1	1	0.016	8433	3.4 (3.3)	22.9 (9.5)	0.05 (0.16)	18.7	3795	1
	2	0.032	8469	3.5 (3.3)	23.2 (9.1)	0.04 (0.17)	19.2	3433	0.9
	3	0.048	8469	3.5 (3.3)	22.0 (8.1)	0.05 (0.19)	19.9	2996	0.79
	4	0.064	8465	3.5 (3.3)	21.1 (7.1)	0.05 (0.22)	21.1	2703	0.71
	5	0.080	8478	3.5 (3.3)	19.8 (6.0)	0.05 (0.26)	21.9	2601	0.69
	6	0.096	8480	3.5 (3.3)	18.2 (4.8)	0.06 (0.33)	23.0	2243	0.59
	7	0.112	8483	3.5 (3.3)	16.6 (3.8)	0.06 (0.41)	24.2	2000	0.53
	8	0.128	8508	3.5 (3.3)	15.0 (2.9)	0.07 (–)	25.9	1817	0.48
NAT2	1	0.034	8484	3.4 (3.3)	13.2 (4.0)	0.11 (0.33)	19.0	2245	1
	2	0.068	8496	3.3 (3.2)	11.0 (2.7)	0.14 (0.45)	20.1	1743	0.78
	3	0.102	8494	3.3 (3.2)	9.8 (1.9)	0.16 (–)	21.8	1431	0.64
	4	0.136	8510	3.3 (3.2)	8.7 (1.3)	0.17 (–)	25.0	1235	0.55
	5	0.17	8525	3.3 (3.2)	7.6 (1.0)	0.20 (–)	27.7	911	0.48
ASC1	*	0.016	n/a	n/a	n/a	n/a	n/a	1476	1
	1	0.069	8570	6.7 (6.2)	16.1 (3.7)	0.11 (0.53)	22.2	1140	0.83
	2	0.138	8597	6.7 (6.2)	14.6 (2.4)	0.13 (–)	24.2	730	0.64
	3	0.207	8625	6.7 (6.3)	9.1 (1.0)	0.31 (–)	27.2	241	0.41
ASC2	*	0.016	n/a	n/a	n/a	n/a	n/a	2945	1
	1	0.069	8577	6.8 (6.3)	28.7 (9.8)	0.05 (0.22)	20.1	2488	0.84
	2	0.138	8575	6.8 (6.3)	23.5 (6.5)	0.06 (0.33)	21.7	2156	0.71
	3	0.207	8594	6.8 (6.3)	18.7 (3.3)	0.09 (–)	25.4	1113	0.62
	4	0.276	8625	6.7 (6.3)	11.3 (1.0)	0.21 (–)	28.4	416	0.32
NAT3	1	0.26	8631	6.9 (7.0)	29.8 (16.2)	0.05 (0.11)	19.8	3653	1
	2	0.52	8631	6.9 (7.0)	26.6 (11.7)	0.05 (0.18)	21.5	2979	0.82
	3	0.78	8643	6.7 (6.9)	17.3 (3.6)	0.21 (–)	23.4	2344	0.64
	4	1.04	8606	6.6 (6.8)	11.7 (1.2)	0.36 (–)	25.8	1486	0.41
	5	1.300	8609	6.6 (6.7)	8.6 (0.8)	0.58 (–)	27.0	1108	0.30
	6	1.56	8596	6.6 (6.7)	6.9 (0.5)	0.52 (–)	29.7	619	0.16
ASC3	*	0.26	n/a	n/a	n/a	n/a	n/a	1938	1
	1	0.27	9023	6.9 (6.8)	22.2 (4.3)	0.06 (0.44)	35.5	1899	0.98
	2	0.81	8944	6.9 (6.9)	17.9 (2.1)	0.07 (–)	38.3	1659	0.86
	3	1.08	8979	6.8 (6.8)	16.1 (1.0)	0.10 (–)	41.7	1472	0.76
4	1.31	8948	6.7 (6.8)	13.8 (0.5)	0.2 (–)	41.0	1302	0.68	

sufficient. Rigid-body refinement of the model (without non-protein atoms) against the first data set for each crystal was carried out using *REFMAC5* (Murshudov *et al.*, 1999). The program *ARP/wARP* was then used to add the water molecules to the models, with water placement and removal being iterated with the maximum-likelihood refinement procedure of *REFMAC5*. *COOT* (Emsley & Cowtan, 2004) was then used for manual model building with restrained refinement being completed by iterative cycling between *REFMAC5* and *COOT*, continuing until the crystallographic R value < 0.20 and R_{free} < 0.25.

The program *CAD* was then used to combine the phases from the refined model of data set 1 for each crystal with the structure factors of the sequential data sets from that crystal, and FFT was used to produce $F_{o1} - F_{ox}$ Fourier difference

maps between data sets (where x is any data set other than 1). These Fourier difference maps were thus a combination of the phases derived from the refined model of data set 1 and the measured structure factors of each sequential data set.

All difference map analysis throughout this work was of negative peaks; there were no significant (greater than 3σ) positive peaks observed. This process of map production eliminates any dilution of the differences between data sets that would arise during the process of individual refinement of structures against each of the data sets. This protocol was arrived at after much testing into the method which most conveniently displayed the differences occurring in the protein structure upon irradiation.

3. Results

The data collection statistics for the radioprotectant screening experiments on ascorbate, 1,4-benzoquinone and TEMP are given in Tables 2, 3 and 4, respectively. Figs. 3 to 6 show the relative summed intensity decay, I/I_0 [mean intensity of a data set (I) divided by the mean intensity of the first data set (I_0)], against absorbed dose, with I values being the $\langle I_{\text{mean}} \rangle$ values from the program *SCALA* for native and scavenger crystals. Although the unit-cell volume was plotted, no systematic trends were observed (data not shown), in contrast to results at

cryotemperatures (Murray & Garman, 2002). The Wilson B factors were also monitored and are shown in Tables 2, 3 and 4.

The effectiveness of a scavenger to prolong crystal lifetime was judged by deriving $D_{1/2}$ (the dose that reduced the intensity of the diffraction pattern to 50% of its original value for data set 1) for each of the native and scavenger crystals, and calculating the radioprotectant enhancement factor, $D_e = D_{1/2}(\text{with scavenger})/D_{1/2}(\text{native})$. Difference electron density maps were analysed for specific damage and in particular to investigate disulfide bond susceptibility. A higher sigma (σ) value in these maps indicated a greater extent of damage. The atomic B factors of the refined structures were analysed in order to analyse the increase in disorder of disulfide bonds between data sets.

Table 3

Data statistics from the HEWL crystals NAT4, QUIN1 and QUIN2 collected in-house.

The resolution range in all cases was 40.00–2.00 Å (2.10–2.00 Å outer shell). For all these data sets the completeness was greater than 96%. The asterisks (*) at the beginning of the QUIN1 and QUIN2 entries denote the virtual normalized intensity point at the same dose as for the first data set of NAT4 as described in the text. The (–) sign represents values above 0.6. $\langle I_{\text{mean}} \rangle$ and R_{meas} are defined as in the Table 2 legend.

Crystal	DS	Dose (MGy)	Unique reflections	Multiplicity	$I/\sigma(I)$	R_{meas}	Wilson B value (Å ²)	$\langle I_{\text{mean}} \rangle$	I/I_0
NAT4	1	0.051	8044	3.3 (3.1)	20.2 (8.4)	0.05 (0.17)	20.2	6777	1
	2	0.102	8054	3.4 (3.2)	20.0 (6.9)	0.05 (0.22)	22.6	4321	0.64
	3	0.153	8072	3.4 (3.3)	17.6 (5.0)	0.06 (0.30)	24.3	3583	0.53
	4	0.204	8085	3.4 (3.2)	13.9 (3.1)	0.08 (0.49)	25.2	2795	0.41
	5	0.255	8085	3.4 (3.3)	12.7 (2.1)	0.09 (–)	29.5	2145	0.32
	6	0.306	8100	3.4 (3.2)	10.3 (1.3)	0.12 (–)	30.2	1430	0.21
	7	0.357	8104	3.4 (3.2)	8.5 (0.9)	0.16 (–)	29.1	1179	0.17
QUIN1	*	0.051	n/a	n/a	n/a	n/a	n/a	n/a	1
	1	0.31	8103	6.5 (6.0)	29.1 (11.3)	0.05 (0.16)	19.8	2628	0.82
	2	0.62	8116	6.7 (6.2)	29.0 (9.9)	0.05 (0.19)	21.8	2579	0.81
	3	0.93	8111	6.7 (6.3)	26.9 (7.5)	0.05 (0.26)	23.4	2181	0.68
	4	1.24	8134	6.7 (6.2)	22.0 (4.2)	0.07 (0.47)	25.1	1741	0.55
	5	1.55	8144	6.6 (6.1)	15.2 (1.4)	0.14 (–)	29.8	1113	0.35
	6	1.86	8168	6.3 (5.8)	7.4 (0.4)	0.40 (–)	12.2	493	0.15
QUIN2	*	0.051	n/a	n/a	n/a	n/a	n/a	n/a	1
	1	0.32	8106	6.6 (6.1)	19.6 (6.2)	0.09 (0.32)	15.4	2220	0.91
	2	0.64	8105	6.7 (6.2)	20.3 (6.2)	0.09 (0.36)	19.3	2180	0.81
	3	0.96	8108	6.7 (6.2)	19.5 (5.5)	0.09 (0.40)	21.5	1862	0.76

Table 4

Data statistics from the HEWL crystals NAT5, NAT6, TEMP1 and TEMP2 collected in-house.

The resolution range in all cases was 40.00–2.00 Å (2.10–2.00 Å outer shell). For all these data sets the completeness was greater than 96%. The (–) sign represents values above 0.6. $\langle I_{\text{mean}} \rangle$ and R_{meas} are defined as in the Table 2 legend.

Crystal	DS	Dose (MGy)	Unique reflections	Multiplicity	$I/\sigma(I)$	R_{meas}	Wilson B value (Å ²)	$\langle I_{\text{mean}} \rangle$	I/I_0
NAT5	1	0.075	8183	6.6 (6.2)	17.8 (5.1)	0.09 (0.37)	21.5	1962.7	1
	2	0.15	8194	6.7 (6.3)	17.4 (4.4)	0.09 (0.46)	23.7	1408.2	0.72
	3	0.225	8202	6.8 (6.3)	16.1 (3.3)	0.10 (–)	26.1	1191.8	0.61
	4	0.3	8221	6.7 (6.3)	13.4 (2.1)	0.13 (–)	30.4	938.1	0.48
	5	0.375	8244	6.7 (6.3)	10.3 (1.2)	0.18 (–)	32.3	671.2	0.34
	6	0.45	8279	6.7 (6.3)	7.4 (0.6)	0.29 (–)	33.1	469.2	0.24
NAT6	1	0.039	8035	3.2 (3.1)	11.9 (2.6)	0.12 (0.48)	21.6	2602.9	1
	2	0.078	8039	3.2 (3.1)	11.7 (2.3)	0.12 (0.54)	22.6	2357.3	0.91
	3	0.117	8028	3.2 (3.1)	11.1 (2.0)	0.13 (–)	24.2	2258.1	0.87
	4	0.156	8035	3.2 (3.1)	10.2 (1.6)	0.14 (–)	26.1	1863.9	0.72
	5	0.195	8054	3.2 (3.1)	9.4 (1.2)	0.15 (–)	27.9	1684.2	0.63
	6	0.234	8074	3.2 (3.1)	8.5 (1.0)	0.17 (–)	29.2	1370.3	0.53
	7	0.273	8062	3.2 (3.0)	7.3 (0.8)	0.20 (–)	29.4	1022.5	0.39
TEMP1	1	0.073	8215	6.7 (6.2)	20.4 (5.6)	0.07 (0.36)	22.8	2084.7	1
	2	0.146	8232	6.8 (6.3)	18.0 (4.0)	0.09 (0.52)	25.2	1585.8	0.76
	3	0.219	8264	6.7 (6.3)	13.5 (1.8)	0.14 (–)	28.5	1209.0	0.58
	4	0.292	8364	6.7 (6.1)	8.2 (0.6)	0.48 (–)	32.4	723.1	0.35
TEMP2	1	0.065	8096	3.3 (3.2)	11.6 (2.7)	0.09 (0.50)	23.6	1838.9	1
	2	0.13	8105	3.3 (3.2)	10.7 (2.2)	0.11 (–)	25.6	1600.9	0.87
	3	0.195	8150	3.4 (3.3)	9.3 (1.4)	0.14 (–)	28.1	1318.2	0.72
	4	0.26	8035	3.4 (3.3)	8.0 (1.0)	0.17 (–)	32.1	1083.0	0.59
	5	0.325	8177	3.3 (3.2)	6.2 (0.6)	0.24 (–)	29.5	831.6	0.45

Following the analysis of the above parameters, it was found that ascorbate was an effective radioprotectant at 293 K (Fig. 3). The $D_{1/2}$ value for NAT1 was 0.125 MGy and the average for ASC1 ($D_{1/2} = 0.17$ MGy) and ASC2 ($D_{1/2} = 0.22$ MGy) was 0.2 MGy, giving a D_e value of 1.6; ascorbate

(Table 2) which showed that for the same absorbed dose the ascorbate co-crystals exhibited lower increases.

The change in the average atomic B factors for cysteine residues involved in disulfide bonds was also analysed for the refined structures derived from the NAT1 and ASC1 data and

thus appears to offer a 1.6-fold increase in tolerated dose. Note that since NAT2 was collected at twice the dose rate (12.8 Gy s^{−1} compared with 6.4 Gy s^{−1} for NAT1) it was not included in the calculation of D_e . As expected from the room-temperature inverse dose rate effect (Southworth-Davies *et al.*, 2007), it showed a higher $D_{1/2}$, but, since the first data set for NAT2 had a larger absorbed dose than that for NAT1, the normalization of these data for direct comparison of $D_{1/2}$ is problematic, since, as mentioned above, extrapolating the exponential fit to the NAT2 data back to the NAT1 data set 1 dose could not be carried out with accuracy.

For the high dose rate measurements (2800 Gy s^{−1}) collected at the ESRF (Fig. 4), values for $D_{1/2}$ of 0.9 MGy (NAT3) and 2.2 MGy (ASC3) were observed, giving a D_e value of 2.4. For NAT3, the inverse dose rate effect results in a $D_{1/2}$ value seven times higher than that for NAT1, and a $D_{1/2}$ value that is 11 times higher for ASC3 than for the average of ASC1 and 2. The crystals were both 0.2 mm in each dimension, whereas the beam was 0.1 mm square, so that a new previously un-irradiated part of the crystal was rotated into the beam during the experiment. Since *RADDOSE* assumes a stationary evenly irradiated crystal, this gives a systematic overestimate of the dose of approximately 6% (Barker, 2008). The dose rate stated above has been corrected for this effect.

Further evidence for the protective effect of ascorbate came from analysing the increase in Wilson B factors

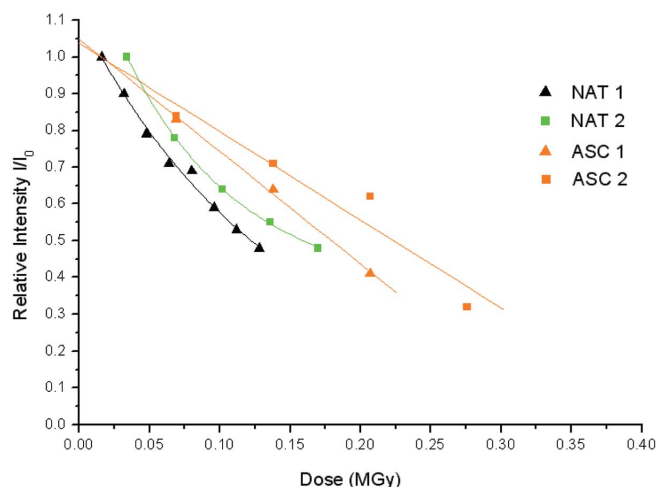


Figure 3

Relative summed intensity of successive data sets plotted against dose for the NAT1, NAT2, ASC1 and ASC2 HEWL crystals. The data were collected in-house at dose rates of 6.0, 12.8, 6.4 and 6.4 Gy s⁻¹, respectively. Of particular note is the exponential decay of the intensity of the native crystals with dose, compared with the linear decay of the scavenger co-crystals.

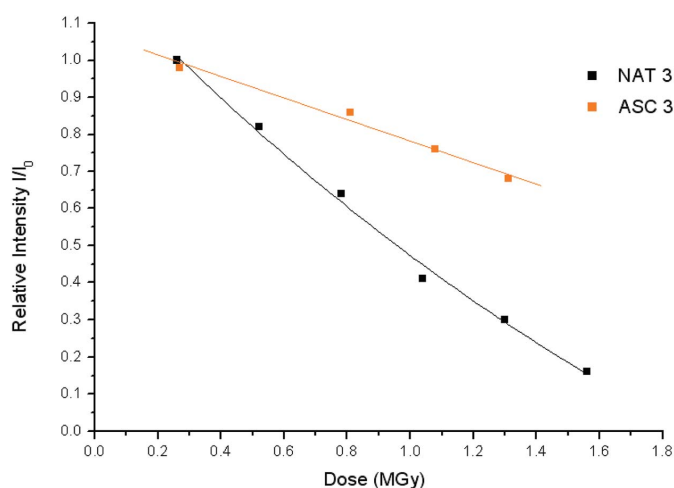


Figure 4

Relative summed intensity of successive data sets plotted against dose for the NAT3 and ASC3 crystals. The data were collected at the ESRF at a dose rate of 2800 Gy s⁻¹. As for the data shown in Fig. 3, the intensity decay of the native crystal is exponential with dose, compared with linear decay for the scavenger co-crystal.

found to be 63% and 13.5%, respectively, further supporting the efficacy of ascorbate.

The difference electron density map ($F_{o1} - F_{ox}$) analysis of the σ values for the disulfide bonds in HEWL (data not shown) showed that in general the ascorbate co-crystal suffered less severe damage than did the native. Conversely, those from ASC3 appeared to show slightly greater damage to the disulfide bonds than for NAT3. This observation is difficult to reconcile with the fact that ascorbate significantly reduces the rate of the relative summed intensity decay with dose for ASC3 and this requires further investigation at high dose rates. However, the electron density maps calculated from all the room-temperature data set decay series are much noisier than those from decay series taken at 100 K owing to the faster

Table 5

Coefficients from *ORIGIN* fits of exponential and linear functions to the data from crystals of native and of those of the two effective scavengers (ASC and QUIN).

n/a signifies that *ORIGIN* was unable to produce an error for the fitted parameters.

Sample	Exponential $y = y_0 + A_1 \exp(-x/t_1)$	Linear $y = A + Bx$
NAT1	$y_0 = 0.054 \pm 0.239$ $A_1 = 1.053 \pm 0.215$ $t_1 = 0.143 \pm 0.052$	$A = 1.039 \pm 0.021$ $B = -4.55 \pm 0.26$
NAT2	$y_0 = 0.354 \pm 0.201$ $A_1 = 0.964 \pm 0.170$ $t_1 = 0.084 \pm 0.058$	$A = 1.03 \pm 0.077$ $B = -3.35 \pm 0.58$
ASC1	$y_0 = -6914.8 \pm \text{n/a}$ $A_1 = 6915.8 \pm \text{n/a}$ $t_1 = 2240.3 \pm \text{n/a}$	$A = 1.05 \pm 0.07$ $B = -3.09 \pm 0.42$
ASC2	$y_0 = -1333.6 \pm 1.60931 \times 10^6$ $A_1 = 1334.7 \pm 1.60931 \times 10^6$ $t_1 = 492.6 \pm 594223.8$	$A = 1.085 \pm 0.078$ $B = -2.71 \pm 0.33$
NAT3	$y_0 = -1.25 \pm 1.01$ $A_1 = 2.48 \pm 0.97$ $t_1 = 2.72 \pm 1.54$	$A = 1.154 \pm 0.033$ $B = -0.658 \pm 0.032$
ASC3	$y_0 = -1342.9 \pm \text{n/a}$ $A_1 = 1344.0 \pm \text{n/a}$ $t_1 = 4553.8 \pm \text{n/a}$	$A = 1.08 \pm 0.08$ $B = -0.295 \pm 0.080$
NAT4	$y_0 = 0.00443 \pm 0.0934$ $A_1 = 1.245 \pm 0.097$ $t_1 = 0.1802 \pm 0.0476$	$A = 0.827 \pm 0.042$ $B = -1.909 \pm 0.138$
QUIN1	$y_0 = -1785.22 \pm 1.95 \times 10^6$ $A_1 = 1786.27 \pm 1.965 \times 10^6$ $t_1 = 3990.10 \pm 4.39 \times 10^6$	$A = 1.028 \pm 0.0463$ $B = -0.434 \pm 0.039$
QUIN2	$y_0 = -224.62 \pm \text{n/a}$ $A_1 = 245.62 \pm \text{n/a}$ $t_1 = 1049.04 \pm \text{n/a}$	$A = 1.00 \pm 0.069$ $B = -0.234 \pm 0.992$

decay during one data set and the faster loss in overall crystal order. The maps are hence harder to interpret.

However, by far the most striking and surprising feature of the ascorbate results displayed in Figs. 3 and 4 is the dramatic alteration in the behaviour of the dose dependence upon introduction of the scavenger, with native crystals showing first-order intensity decay with dose and ascorbate co-crystals zeroth-order intensity decay (see §4) with dose. The native and ascorbate intensity decay data were fitted using the *ORIGIN* software package to both straight line and exponential functions, and the resulting parameters and their errors are detailed in Table 5. It can be seen from the relative magnitudes of the coefficients for the exponential fits to the native data and putative exponential fits to the scavenger data that the difference between the exponential and linear dependence is clear. The ASC scavenger data, when fitted with an exponential decay function, give coefficients in the thousands with either enormous or no determinable error ('n/a') in an attempt to produce an exponential fit for data which are best described by a linear function, whereas the native crystals give coefficients describing a visibly exponential function.

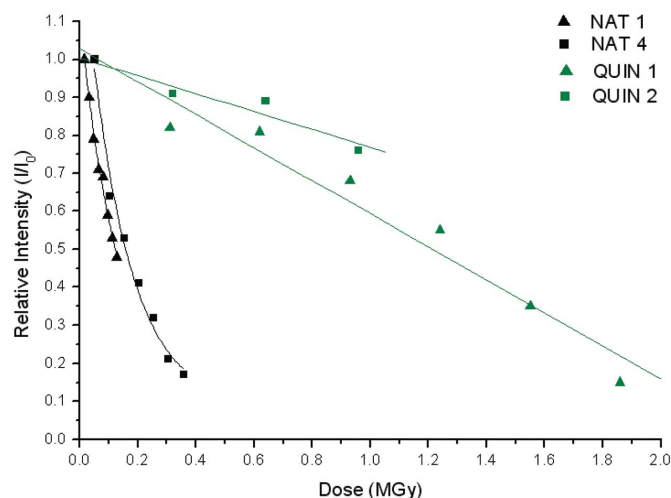


Figure 5

Relative summed intensity of successive data sets plotted against dose for the NAT1, NAT4, QUIN1 and QUIN2 soaked HEWL crystals. The data were collected in-house at dose rates of 6.0, 5.7, 6.4 and 6.0 Gy s⁻¹, respectively.

Addition of the scavenger 1,4-benzoquinone also proved an effective damage mitigation strategy at 293 K. The data statistics are shown in Table 3 and the intensity decay with dose is plotted in Fig. 5, from which it can be seen that the $D_{1/2}$ value for the native crystals (NAT1: 0.125 MGy; NAT4: 0.15 MGy) was 0.14 MGy and for the 1,4-benzoquinone soaked crystal (QUIN1: 1.25 MGy; QUIN2: too few points to include) was 1.25 MGy, thus giving a D_e value of 8.9. This protective effect is again reinforced by noting the change in Wilson B factors (Table 3), which is 50% for NAT4 and 40% for QUIN2 after doses of 0.31 MGy and 0.62 MGy (*i.e.* double), respectively. Similarly, inspection of the change in the average atomic B factors for cysteine residues (data not shown) showed that the value for native crystals was approximately twice that of 1,4-benzoquinone soaked crystals after an equivalent dose.

Analysis of electron density maps revealed that, even with double the dose, the susceptible residues of the structures derived from the 1,4-benzoquinone-soaked crystals still showed significantly less damage (and some disulfides showed no damage at all; data not shown) compared with the native structures, and also in general less damage than the ascorbate co-crystal structures.

Once again the striking change in intensity decay with dose from first to zeroth order was observed in the scavenger containing crystals. The data were fitted to linear and exponential functions as described above and showed similar behaviour: large coefficients with either enormous or undetermined errors on them for exponential functions with the two QUIN intensity decay series (Table 5).

In contrast to the above results with ascorbate and 1,4-benzoquinone, the experiments with TEMP were inconclusive (Fig. 6). The $D_{1/2}$ values suggested that there is very little difference between $D_{1/2}$ for native (average 0.25 MGy; NAT5: 0.266 MGy; NAT6: 0.240 MGy) and TEMP-soaked (average 0.275 MGy; TEMP1: 0.230 MGy; TEMP2: 0.305 MGy) crys-

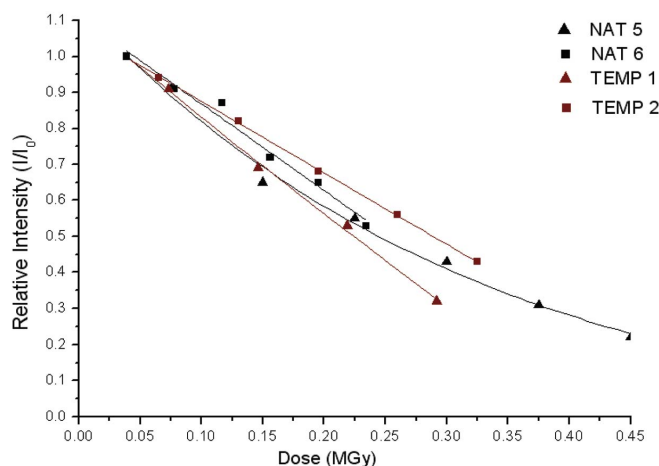


Figure 6

Relative summed intensity of successive data sets plotted against dose for the NAT5, NAT6, TEMP1 and TEMP2 soaked HEWL crystals. The data were collected in-house at dose rates of 4.6, 4.8, 4.5 and 4.8 Gy s⁻¹, respectively. The scavenger is ineffective and all the intensity decays with dose show exponential forms.

Als. Additionally, the analysis of B factors showed no significant difference and the average cysteine B values rose by 71% and 108% for NAT5 and TEMP2, respectively, indicating that TEMP may actually exacerbate radiation damage. Thus although some further experiments with TEMP and other types of crystal might be useful, it is clear that any effects on HEWL are small.

Also, unlike ascorbate and 1,4-benzoquinone, TEMP did not induce a change in the dependence of intensity loss with dose, with native crystals and TEMP-soaked crystals both displaying first-order decay.

As mentioned above, the electron density difference maps were analysed for the relative susceptibilities of residues to damage, in particular to disulfide bonds. Although at cryotemperatures damage to other residues such as glutamate and aspartate is also common, no specific damage to these residues was observed here. Indeed, at cryotemperatures, the damage to disulfides occurs at much higher σ levels compared with those seen in this study, since at 100 K the global crystal order is retained for much longer. Thus specific damage is much more difficult to see clearly in electron density maps created from room-temperature data, and no systematic trends in susceptibility were clear for the scavenger compared with native structures for ascorbate, 1,4-benzoquinone or TEMP treated crystals.

Ravelli & McSweeney (2000) suggested that susceptibility at 100 K was correlated with solvent accessibility, and this is supported by other evidence (Weik *et al.*, 2000; Burmeister, 2000). However, work on wing bean chymotrypsin (Ravelli & McSweeney, 2000) and halophilic malate dehydrogenase (Fioravanti *et al.*, 2007) suggests that solvent accessibility does not explain the trends, and that other factors such as proximity to active sites and sites of crystal contact may be important. This issue is still to be resolved, but the room-temperature disulfide bond susceptibility seen here appeared to show no reproducible trends.

4. Discussion

Although our results are for only a limited number of samples for each scavenger, and are of a preliminary nature, clearly the most important finding of this work is the dramatic change in the dose dependence of the diffracted intensity, from first to zeroth order, upon addition of scavenger to the crystals. Both the effective radioprotectants, ascorbate and 1,4-benzoquinone, exhibit this phenomenon. Substantial alteration of the radiation chemistry has obviously taken place; although the amount of energy deposited in the crystal is the same, the results of that energy deposition are different. The observed exponential intensity decay (first order in dose) at room temperature can be interpreted as being a result of the participation of secondary damage processes arising from radicals produced in the environment of the protein. At room temperature, such radical species diffuse readily and can widely access susceptible sites on the protein, compounding primary damage caused by energy deposition events in the protein and the subsequently generated secondary electrons.

The dose dependence of the intensity is first order at room temperature because energy deposited in the surrounding medium creates radicals which subsequently attack otherwise undamaged protein. Hence, the rate of decay is proportional to the amount of undamaged material remaining, the definition of a first-order process. The effect of scavengers is to intercept these radicals in the environment of the protein, thus mitigating this component of the damage and changing the dose dependence to zeroth order. Such zeroth-order decay of the total diffracted intensity is routinely observed at cryotemperatures without the addition of scavengers.

This low-temperature zeroth-order dose dependence of the intensity is due to direct damage to the protein, *i.e.* the primary absorption event and its secondary consequences. The flood of secondary electrons produced by the initially released photoelectron appear to be mobile at 100 K in the vitreous solid, and migrate to specific sinks with high electron affinity such as disulfide bonds, rather than leading to overall diffraction degradation. The intensity decay reflects the increasing disorder of the protein molecules, resulting in a decrease in coherent X-ray scattering. The extent of the induced disorder is directly proportional to the energy lost by the X-ray beam in the crystal (*i.e.* the dose resulting in both primary and secondary damage); the extent of damage with dose does not depend on the amount of undamaged material remaining (the definition of a zeroth-order process). Only very weak dose-rate dependence on this intensity decay has been observed at cryotemperatures (Sliz *et al.*, 2003; Leiros *et al.*, 2006; Owen *et al.*, 2006) with higher dose rates giving slightly reduced $D_{1/2}$ values. This is further evidence of the postulated dominance of direct damage in the general loss of crystal diffraction at cryotemperatures, and that specific structural damage is due to direct and indirect secondary damage [since some dose dependence has been reported for this component (Leiros *et al.*, 2006)].

Both ascorbate and 1,4-benzoquinone effectively intercept hydroxyl radicals with $k_{\text{OH}} = 8 \times 10^9 \text{ M}^{-1} \text{ s}^{-1}$ and $1.2 \times$

$10^9 \text{ M}^{-1} \text{ s}^{-1}$, respectively, in aqueous solution (Buxton *et al.*, 1988) producing much less reactive species of lower mobility. They both also scavenge electrons but with rates of $k_{e-(\text{aq})} = 3.0 \times 10^8 \text{ M}^{-1} \text{ s}^{-1}$ (Schuler *et al.*, 1974) and $1.2 \times 10^{10} \text{ M}^{-1} \text{ s}^{-1}$ (Milosavljevic & Micic, 1978), for ascorbate and 1,4-benzoquinone, respectively. The reaction rates given are representative of those expected in protein crystals. Since both scavengers induce altered dose dependencies in the observed diffracted intensities, the interaction of the OH^\bullet radical with crystal constituents is clearly implicated as the major source of the first-order component of the dose dependence. This also sheds light on the zeroth-order dose dependence observed at 100 K, since OH^\bullet radicals are thought not to be mobile below 110 K (M. Sevilla, private communication) whereas electrons are known to be able to move at 77 K (Jones *et al.*, 1987).

The ratios of scavenging rate constants for electrons and OH^\bullet radicals are very different for 1,4-benzoquinone and ascorbate, being $k_{e-(\text{aq})}/k_{\text{OH}} = 10$ and 0.037, respectively. The increased efficiency of 1,4-benzoquinone as an electron scavenger is a possible explanation of its higher efficacy as a radioprotectant of HEWL crystals.

Specific structural damage to disulfides was observed in the ascorbate data derived electron density maps (although to a lesser extent than in the native structures), but significantly less damage was observed to those from 1,4-benzoquinone containing crystals, where electrons generated in the solvent are being more effectively scavenged. This confirms that specific structural damage to disulfides, widely observed under cryoconditions, is definitely not attributable to mobile OH^\bullet radicals, but clearly electrons are implicated. Murray & Garman (2002) observed reduced specific damage to disulfide bonds at cryotemperatures in ascorbate-soaked crystals of lysozyme, which, since the OH^\bullet radicals are immobile, implies that the electron scavenging capacity of ascorbate is the effective agent at cryotemperatures.

5. Conclusions

The preliminary results presented above show that both ascorbate and 1,4-benzoquinone are effective in significantly increasing the dose that can be tolerated during data collection from room-temperature lysozyme crystals, the former by a factor of ~ 2 and the latter by a factor of ~ 9 at the dose rates used (5.7 Gy s^{-1} to 6.4 Gy s^{-1}). In both instances a 1 M scavenger was used, with ascorbate being introduced by co-crystallization (to give a concentration of around 0.5 M in the co-crystals) and 1,4-benzoquinone by soaking in 1 M scavenger solution, with soaking times of three or seven days, again giving around 0.5 M concentration in the crystals. The analysis of Wilson and atomic B factors also generally supported the above conclusions.

For the ascorbate ESRF higher dose rate experiments (2800 Gy s^{-1}), the in-house results were reproduced, but the crystals tolerated a much higher dose owing to the inverse dose rate effect already reported (Southworth-Davies *et al.*, 2007). Thus the scavengers are able to mediate their effect

over the remarkably large dose rate range of 6 Gy s^{-1} to 2800 Gy s^{-1} .

The results seem to be explained by the fact that both ascorbate and 1,4-benzoquinone can scavenge both OH^\bullet radicals and solvated electrons, albeit with different relative efficiencies.

Thus it is concluded that ascorbate, and particularly 1,4-benzoquinone, are promising candidate molecules for testing on other protein systems at room temperature, since they significantly increased the $D_{1/2}$ values for lysozyme crystals.

However, the addition of scavenger also strikingly altered the dose dependence of the intensity decay. Other room-temperature observations of intensity decay (Blake & Phillips, 1962; Hendrickson *et al.*, 1973; Fletterick *et al.*, 1976; Southworth-Davies *et al.*, 2007; Sygusch & Allaire, 1988) have all shown first-order exponential decay, whereas both the ascorbate and 1,4-benzoquinone induce a linear intensity decay, indicating a zeroth-order process. The effective scavenging of OH^\bullet radicals is strongly implicated in this modification of the dose dependence of the decay.

Our results shed insight into the mechanism of the protective action of ascorbate and quinone at room temperature, and our preliminary findings on the altered functional form of the intensity decay with dose have allowed us to postulate a mechanism for radiation damage under these conditions. Both these aspects of radiation damage in crystallography are worthy of further investigation to develop mitigation strategies and to clarify the mechanisms of radiation chemistry involved at both room and cryotemperatures.

We thank Elizabeth Armstrong and Ed Lowe for their valuable assistance with data collection, Mike Sevilla for useful discussions on the possible scavenging mechanisms, and Andrew Leslie for suggesting various methods of error estimation on data processing statistics. We gratefully acknowledge access to beam time at the ESRF under Radiation Damage BAGs MX666 and 812. The Notre Dame Radiation Laboratory is supported by Basic Energy Sciences at the US Department of Energy (this is document number NDRL-4792). This work was supported by the Biotechnology and Biological Sciences Research Council with a CASE studentship to RSD and by an EU Sixth Framework Programme 'TotalCryst' grant to KSP. We dedicate this paper to Myrtle, the long-serving Rigaku RU200H X-ray generator installed on 1 June 1987 and decommissioned on 14 August 2008, on which some of the data presented here were collected. She helped to solve over 50 new macromolecular structures and gave data for over 250 ligand soaks, achieving >90% uptime for her clock lifetime of 143313 h.

References

Armstrong, D. A. (1990). *Applications of Pulse Radiolysis for the Study of Short-Lived Sulfur Species, Sulfur-Centered Reactive Intermediates in Chemistry and Biology*, edited by K. Chatgililoglu and K.-D. Asmus, pp. 121–134. New York: Plenum.

Armstrong, E. (2008). Part II thesis, Oxford University, England. (Unpublished work.)

Barker, A. (2008). Part II thesis, Oxford University, England. (Unpublished work.)

Betts, S. (2003). Part II thesis, Oxford University, England. (Unpublished work.)

Blake, C. C. F. & Phillips, D. C. (1962). *Biological Effects of Ionizing Radiation at the Molecular Level*, pp. 183–191. Vienna: International Atomic Energy Agency.

Burmeister, W. P. (2000). *Acta Cryst.* **D56**, 328–341.

Buxton, G., Greenstick, C., Helman, W. & Ross, A. (1988). *J. Phys. Chem. Ref. Data*, **17**, 513–886.

Cascio, D., Williams, R. & McPherson, A. (1984). *J. Appl. Cryst.* **17**, 209–210.

Collaborative Computational Project, Number 4 (1994). *Acta Cryst.* **D50**, 760–763.

Emsley, P. & Cowtan, K. (2004). *Acta Cryst.* **D60**, 2126–2132.

Evans, P. (2006). *Acta Cryst.* **D62**, 72–82.

Fioravanti, E., Vellieux, F. M. D., Amara, P., Madern, D. & Weik, M. (2007). *J. Synchrotron Rad.* **14**, 84–91.

Fisher, M. & Devlin, J. P. (1995). *J. Phys. Chem.* **99**, 11584–11590.

Fletterick, R. J., Sygusch, J., Murray, N. & Madsen, N. B. (1976). *J. Mol. Biol.* **103**, 1–13.

French, S. & Wilson, K. (1978). *Acta Cryst.* **A34**, 517–525.

Garman, E. (1999). *Acta Cryst.* **D55**, 1641–1653.

Garman, E. F. & Owen, R. L. (2006). *Acta Cryst.* **D62**, 32–47.

Garman, E. F. & Schneider, T. R. (1997). *J. Appl. Cryst.* **30**, 211–237.

Gonzalez, A. & Nave, C. (1994). *Acta Cryst.* **D50**, 874–877.

Gonzalez, A., Thompson, A. & Nave, C. (1992). *Rev. Sci. Instrum.* **63**, 1177–1180.

Haas, D. J. & Rossmann, M. G. (1970). *Acta Cryst.* **B26**, 998–1004.

Hendrickson, W. A., Love, W. E. & Karle, J. (1973). *J. Mol. Biol.* **74**, 331–361.

Hope, H. (1988). *Acta Cryst.* **B44**, 22–26.

Howell, P. L. & Smith, G. D. (1992). *J. Appl. Cryst.* **25**, 81–86.

Jones, G. D. D., Lea, J. S., Symons, M. C. R. & Taiwo, F. A. (1987). *Nature (London)*, **330**, 772–773.

Kalinin, Y., Kmetko, J., Bartnik, A., Stewart, A., Gillilan, R., Lobkovsky, E. & Thorne, R. (2005). *J. Appl. Cryst.* **38**, 333–339.

Kauffmann, B., Weiss, M. S., Lamzin, V. S. & Schmidt, A. (2006). *Structure*, **14**, 1099–1105.

King, M. V. (1958). *Nature (London)*, **181**, 263–264.

Lange, M., Weiland, B. & Hüttermann, J. (1995). *Int. J. Radiat. Biol.* **68**, 475–486.

Leiros, H.-K. S., Timmins, J., Ravelli, R. B. G. & McSweeney, S. M. (2006). *Acta Cryst.* **D62**, 125–132.

Leslie, A. G. W. (2006). *Acta Cryst.* **D62**, 48–57.

McGeehan, J., Ravelli, R. B. G., Murray, J. W., L., Owen, R. L., Cipriani, F., McSweeney, S., Weik, M. & Garman, E. F. (2009). *J. Synchrotron Rad.* **16**, 163–172.

Milosavljevic, B. H. & Micic, O. I. (1978). *J. Phys. Chem.* **82**, 1359–1362.

Murray, J. & Garman, E. (2002). *J. Synchrotron Rad.* **9**, 347–354.

Murray, J. W., Garman, E. F. & Ravelli, R. B. G. (2004). *J. Appl. Cryst.* **37**, 513–522.

Murshudov, G. N., Vagin, A. A., Lebedev, A., Wilson, K. S. & Dodson, E. J. (1999). *Acta Cryst.* **D55**, 247–255.

O'Neill, P., Stevens, D. L. & Garman, E. F. (2002). *J. Synchrotron Rad.* **9**, 329–332.

Owen, R. L., Holton, J. M., Schulze-Briese, C. & Garman, E. F. (2009). *J. Synchrotron Rad.* **16**, 143–151.

Owen, R. L., Rudino-Pinera, E. & Garman, E. F. (2006). *Proc. Natl Acad. Sci.* **103**, 4912–4917.

Paithankar, K. S., Owen, R. L. & Garman, E. F. (2009). *J. Synchrotron Rad.* **16**, 152–162.

Rao, D. N., Symons, M. C. R. & Stephenson, J. M. (1983). *J. Chem. Soc. Perkin Trans. II*, pp. 727–730.

Ravelli, R. B. G. & Garman, E. F. (2006). *Curr. Opin. Struct. Biol.* **16**, 624–629.

Ravelli, R. B. G. & McSweeney, S. M. (2000). *Structure*, **8**, 315–328.

- Rodgers, D. W. (1997). *Methods Enzymol.* **276**, 183–203.
- Sarma, R. & Zaloga, G. (1975). *J. Mol. Biol.* **98**, 479–484.
- Schuler, M. A., Bhatia, K. & Schuler, R. H. (1974). *J. Phys. Chem.* **78**, 1063–1074.
- Sliz, P., Harrison, S. C. & Rosenbaum, G. (2003). *Structure*, **11**, 13–19.
- Southworth-Davies, R. J. & Garman, E. F. (2007). *J. Synchrotron Rad.* **14**, 73–83.
- Southworth-Davies, R. J., Medina, M. A., Carmichael, I. & Garman, E. F. (2007). *Structure*, **15**, 1531–1541.
- Swartz, H. M. & Swartz, S. M. (1983). *Methods Biochem. Anal.* **29**, 207–323.
- Sygyusch, J. & Allaire, M. (1988). *Acta Cryst.* **A44**, 443–448.
- Symons, M. C. R. (1999). *Prog. React. Kinet. Mech.* **24**, 139–164.
- Teng, T.-Y. (1990). *J. Appl. Cryst.* **23**, 387–391.
- Ward, J. F. (1988). *Prog. Nucl. Acid Res. Mol. Biol.* **35**, 95–125.
- Weik, M., Bergès, J., Raves, M. L., Gros, P., McSweeney, S., Silman, I., Sussman, J. L., Houée-Levin, C. & Ravelli, R. B. G. (2002). *J. Synchrotron Rad.* **9**, 342–346.
- Weik, M., Ravelli, R., Kryger, G., McSweeney, S., Raves, M., Harel, M., Gros, P., Silman, I., Kroon, J. & Sussman, J. (2000). *Proc. Natl Acad. Sci.* **97**, 623–628.
- Zaloga, G. & Sarma, R. (1974). *Nature (London)*, **251**, 551–552.